Interferometric oil-spill detection system

Yen-Chieh Huang, MEMBER SPIE
National Tsinghua University
Department of Electrical Engineering
Hsinchu 30043, Taiwan

Uen-Chin Liang
National Tsinghua University
Department of Atomic Science
Hsinchu 30043, Taiwan

Abstract. Oil spillage in a body of water has been of great environmental concern. We present in this paper an automatic oil-spill detection system, which employs thin-film and wavefront-splitting interference techniques to determine the existence of surface oil or oil drops in water. Two independent automatic decision-making systems have been built to provide a reliable means of oil-spill detection. Initially a LabVIEW™ computer code and a charge-coupled-device camera were employed to discern and monitor the interference fringes generated from oil slicks. The LabVIEW imaging system was then replaced by a compact and low-cost imaging circuit that functions reliably in a buoy with relatively low power consumption.
[DOI: 10.1117/1.1359795]

Subject terms: oil spillage; thin-film interference; wavefront-splitting interference.

Paper 200143 received Apr. 10, 2000; revised manuscript received Aug. 21, 2000; accepted for publication Dec. 5, 2000.

1 Introduction

Oil spillage can occur in numerous locations such as seabed exploration sites, oil refineries, or areas close to oil tanks and pipelines. The loss of oil causes both capital and environmental damage. In particular, the environmental damage often takes a long time to recover. It is desirable to have an automatic oil-spill detection system that monitors oil leaks in the early stage and transmits a suitable warning signal to dispatch a rescue action for repair.

The existing oil-spill detection schemes are mostly in two categories, the scanning type and the fixed-location type. The scanning type, usually satellite-based, monitors a large area of many square kilometers. For example, synthetic aperture radar (SAR) has a large coverage over seawater.[1–4] The SAR imagery previously had some difficulty in distinguishing dark areas and lookalikes from oil spills.[5,6] This problem was recently solved by Schistad Solberg et al.[7] The fixed-location oil spill detectors are often buoyantly situated or anchored. Sometimes the buoy is set adrift but its coordinates are controlled by the Global Positioning System. These fixed-type oil-spill detectors monitor oil spills by chemical[8] or optical means. Chemical reactions usually cause pollution themselves, and chemicals are relatively difficult to maintain. Among the optical means, the generation of UV-induced fluorescence[9] and the change of surface reflectivity on surface oil[10] are the two existing oil-spill detection mechanisms to our knowledge. Unfortunately, all of the existing detection schemes have one or several disadvantages, such as poor reliability, high power consumption, high cost, difficulties in maintenance, and complexity.

The SAR oil spillage detection technique is aimed at large-area monitoring, while fixed-location buoy detectors are suitable for real-time, prompt spillage warning in the deployed area. In this paper we design an early-warning surface-oil detector by using optical interferometric techniques. Unlike the existing optical schemes, the interferometric technique detects the interferometric images formed by thin oil films or by oil droplets. The interferometric image formation is more related to the oil geometry than to its material properties. Integrated into a compact circuit board, this technique is relatively simple, reliable, low-cost, and low-power.

2 Interferometric Techniques

In general, oils in a body of water are of two kinds: those with surface tension smaller or larger than that of water. The former kind spreads itself into a thin oil film above the water surface, whereas the latter often forms an oil drop in water. For example, gasoline spreads itself quickly into a thin film on water, and heavy engine oil sometimes forms droplets. We delineate in the following the interferometric techniques for detecting both types of oil spillage on a water surface.

A thin layer of oil on a water surface may generate rainbow-type interference fringes when viewed under the sun. This phenomenon is often observed in our daily life. It results from the well-known thin-film interference, where the reflected light from the oil surface interferes with that from the water surface below the oil film. Because the sun is a white light source, one observes constructive interference of different colors at different angles. When illuminated by a narrowband coherent light source, like a laser, the interference image is even more pronounced, with alternating bright and dark stripes corresponding to the constructive and destructive interference at that particular wavelength. Thin-film interference occurs only when the refractive index of the film differs from those of the materials sandwiching the film.

Figure 1 illustrates the scattering configuration for our theoretical calculation, wherein monochromatic light is incident from medium 1 on medium 3 with the thin film, medium 2, sandwiched in between. By performing the standard infinite-sum calculation for the successive reflected field,

 0091-3286/2001/$15.00

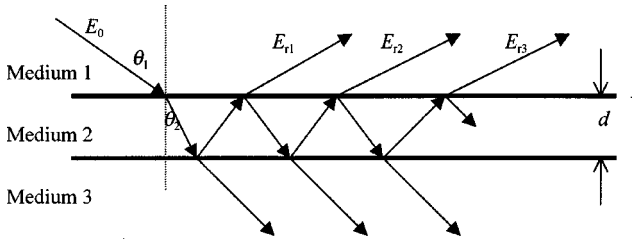

Fig. 1 The configuration for performing the thin-film interference calculation. The three media in this paper are air, oil, and water. The total reflected optical field is the sum of all individual reflected fields, $E_{r1}, E_{r,2}, E_{r,3}$ . . . . Here θ_1 is the incident angle in medium 1, and θ_2 is the refractive angle in medium 2.

$$E_r = E_{r1} + E_{r2} + E_{r3} + \cdots$$

we obtain the reflectance expression,

$$R = \frac{I_r}{I_0} = \frac{\left(\frac{\rho_{23} - \rho_{21}}{1 - \rho_{21}\rho_{23}}\right)^2 + F \sin^2 \frac{\delta}{2}}{1 + F \sin^2 \frac{\delta}{2}}, \tag{1}$$

where $F = 4\rho_{21}\rho_{23}/(1-\rho_{21}\rho_{23})^2$ is the coefficient of finesse, δ is the optical phase difference between successive reflections, and ρ_{mn} is the reflection coefficient when light is incident from medium m to medium n. The phase difference is given by $\delta = (2\pi/\lambda_0)2dn_2 \cos\theta_2$, where λ_0 is the free-space wavelength of the incident light, d is the thin-film thickness, and θ_2 is the refractive angle in medium 2. The refractive angle θ_2 can be found from Snell's law for a known incident angle θ_1 in medium 1. If medium 1 and medium 3 are of the same material and therefore $\rho_{21} = \rho_{23}$, the reflectance in Eq. (1) reduces to the etalon formula[11]

$$R = \frac{I_r}{I_0} = \frac{F \sin^2(\delta/2)}{1 + F \sin^2(\delta/2)}. \tag{2}$$

In the etalon formula, the contrast, or visibility, of the reflected image is always 100%, because the destructive interference reflects no light back to medium 1. However, for the case of three layers, the reflected light from medium 3 cannot completely cancel the light reflected from medium 1 in its destructive phase. Therefore the visibility of the reflection fringes from a thin oil film sandwiched between air and water is not as good as in an etalon, depending on the differences among the refractive indices of the three media. Furthermore, the reflection coefficients ρ_{21} and ρ_{23} are functions of the light polarization, as can be seen from the Fresnel equations.[12] Figure 2 illustrates the reflectance versus the incident angle calculated from Eq. (1) for TM and for TE incident wave. The refractive indices of the three media in our calculation are $n_1 = 1$ (air), $n_2 = 1.1$ (95-octane unleaded gasoline, Chinese Petroleum Corp.), $n_3 = 1.3$ (water). The thickness of the gasoline layer at a certain location varies over the time course of oil spillage, depending on the amount of gasoline in that area. In our

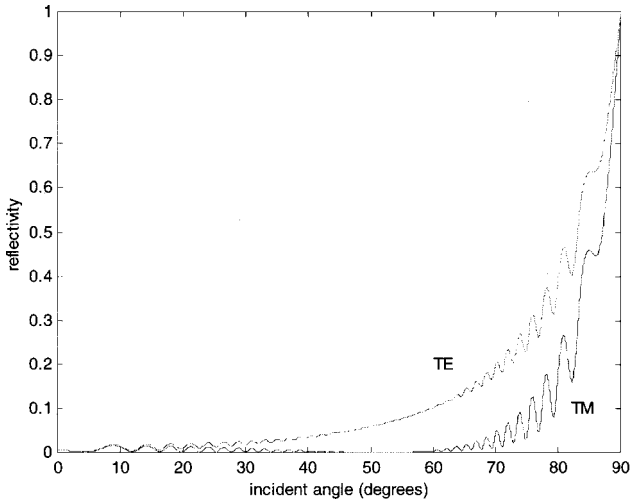

Fig. 2 Thin-film interference fringe intensity versus incident angle for TE and TM incident waves. The refractive indices of the three media are $n_1 = 1$ (air), $n_2 = 1.1$ (95-octane unleaded gasoline, Chinese Petroleum Corp.), $n_3 = 1.3$ (water). The gasoline film thickness is assumed to be 20 μm.

plot we arbitrarily chose a thickness $d = 20$ μm to illustrate a typical situation. The number of interference fringes in Fig. 2 increases with the thickness of the oil layer over a fixed range of the incident angle. For TM-wave incidence, no light is reflected at the Brewster angle near 48 deg. However, it is evident that TM polarization shows more intensity modulation and thus gives better visibility.

When the refractive indices of the oil and water are not very different, the reflectance expression (1) reduces to $R = I_r/I_0 \approx \rho_{21}^2 + 4\rho_{21}\rho_{23} \sin^2(\delta/2)$ with the approximation $\rho_{23} \approx 0$ and $|\rho_{21}| \gg |\rho_{23}|$. It is straightforward to show that the visibility becomes $V = I_{r,\max} - I_{r,\min}/I_{r,\max} + I_{r,\min} \approx 2|\rho_{23}/\rho_{21}| \approx 0$. Therefore the thin-film interference fringes may not be discernible by an image recording apparatus when the refractive indices of the second and third media are very close to each other. However, in our experiment we observed highly visible interference fringes, when medium 2 is Castrol 10W-60 engine oil with refractive index $n = 1.4$ and medium 2 is water with refractive index $n = 1.3$. The interference fringes result from the division of the laser wavefront at the oil-water interface, as Fig. 3 illustrates. In particular, some oil has a larger surface tension, forming a curved surface at the edge immediately next to a water flat. The radius of curvature of the curved surface, typically less than a millimeter, is much smaller than that of the laser wavefront, because in our case the laser waist is about 14 cm from the water surface. Therefore, the reflected wave is approximately a superposition of a plane wave and a wave with its wavefront conforming to the curved oil edge. These two waves form an interference pattern in the far field. Because the refractive indices of the oil and water are close to each other, the visibility of the interference pattern is nearly 100%. The mechanism is in fact similar to wavefront-splitting interference.[13] In our case a curved wavefront and a nearly plane wavefront, derived from a single laser wavefront at the interface between oil and water, interfere with each other in the far field.

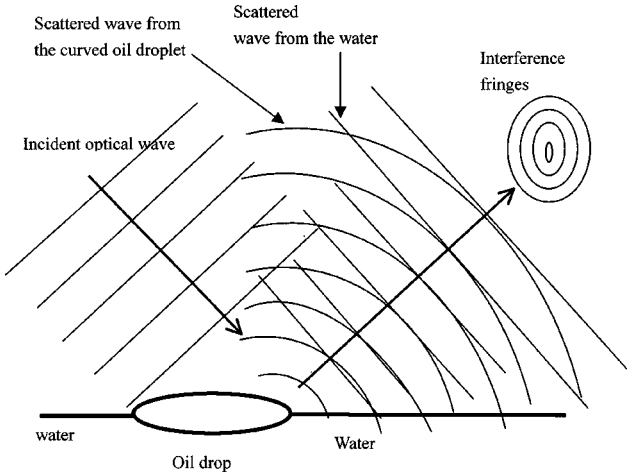

Fig. 3 Illustration of wavefront-splitting interference resulting from an oil drop. The laser wavefront is split into a plane wavefront originating from the water and a curved wavefront originating from the oil drop. The two waves interfere with each other in the far field.

For oils with a small surface tension, the same technique applies as well. When oil spreads from a high-concentration area over a water surface, it moves with a curved edge in the depth direction and eventually forms a thin oil layer on the water. As an early warning system, this technique is capable of picking up the interference signal at the initial phase of oil spread. Moreover, surface oil is often broken into many droplets or islands in a shaky water environment, and those oil droplets and islands can be the scattering sources for wavefront-splitting interferometry.

The interference can be best appreciated by adding a plane wave and a spherical wave. Figure 4 shows this simplified configuration, where a plane wave is normally incident on a spherical oil bump of radius r above a water surface. In the far field $z=d$, the scattered field is approximately the superposition of a plane wave and a spherical wave, originating at a distance r_0 below the water surface at $z=0$. At large d, the spherical wave can be approximated by a paraboloidal wave,[14] given by the phasor representation

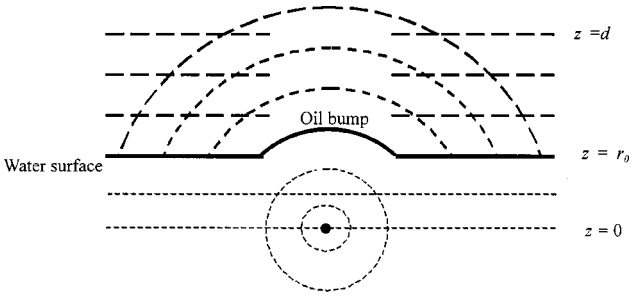

Fig. 4 The scattering configuration for modeling wavefront- splitting interference. A plane wave is incident normally in the $-z$ direction onto a oil bump. The reflected wave is approximately a superposition of a plane wave and a spherical wave. The thick dashed lines above the water surface represent the wavefronts of the plane wave and the spherical wave. The thin dashed lines are the virtual wavefronts originating from the spherical center of the oil bump.

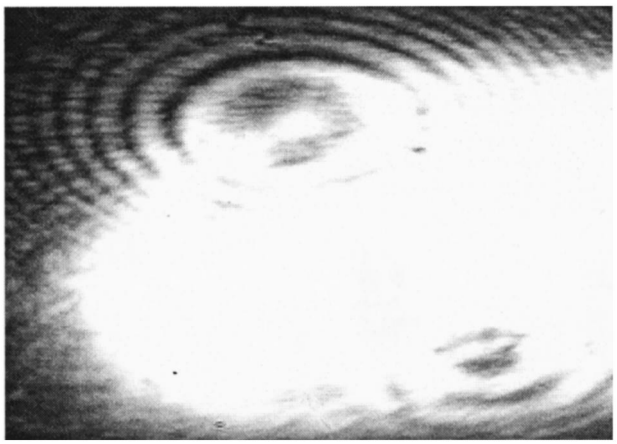

Fig. 5 A typical wavefront-splitting interference image resulting from an oil drop. The interference pattern reflects the symmetry of the oil drop.

$$E_s=\sqrt{I_0}\,\exp\left(-jkd-jk\frac{r^2}{2d}\right), \tag{3}$$

where I_0 is the normalized intensity of the laser at $z=d$, r is the distance from the z axis, and $k=2\pi/\lambda$ is the wave number. Assuming that the plane-wave field at $z=d$ has a comparable intensity, one obtains its phasor representation

$$E_p=\sqrt{I_0}\,\exp(-jkd). \tag{4}$$

The total intensity at $z=d$ is therefore

$$I(z=d)=|E_s+E_p|^2=4I_0\,\cos^2\left(k\frac{r^2}{4d}\right). \tag{5}$$

Equation (5) predicts the Nth constructive interference fringe at the radius

$$r_N=\sqrt{2d\lambda N}. \tag{6}$$

The constructive interference at $z=d$ forms a series of bright rings with decreasing separation in r. For example, to have $r_1=1$ mm for $\lambda=670$ nm, d must be about 75 cm. If the image plane is 30 cm above the water surface, the radius of curvature of the oil bump is 45 cm. In our experiment, we frequently observed those highly visible rings with their shape mimicking the oil drop. Figure 5 shows a typical image, in which the laser incident angle is 80 deg with respect to the normal to the water surface, the laser wavelength is 670 nm, and the distance between the water surface and the image plane is 30 cm. The oil drop was made of Castrol 10-60W engine oil with a measured refractive index of 1.4.

3 Image Processing and Discerning

Figure 6 illustrates the experimental setup, where a 670-nm-wavelength diode laser module (made by HC Photonics Co. Ltd.) is the light source, an image-extraction system records the interference fringes, and the image-processing system determines whether oil spillage exists. Since the oil

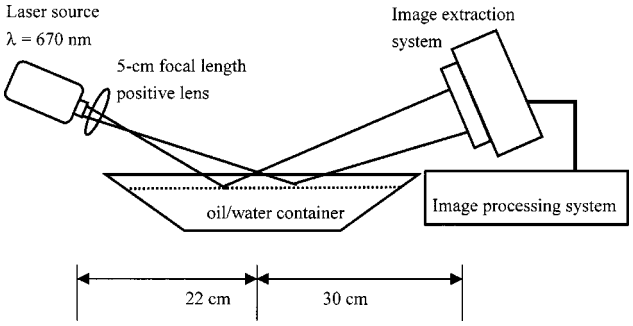

Fig. 6 The experimental setup of our measurement. The image extraction system and the image processing system are initially a CCD camera and a computer, and later become a linear sensor array and a home-made discerning circuit.

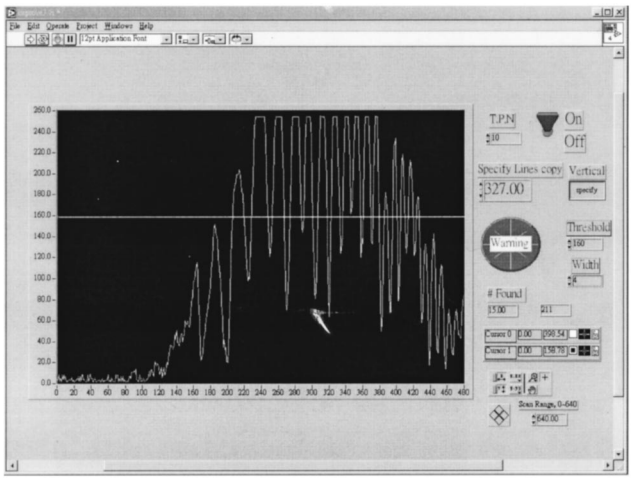

Fig. 7 A typical output of our CCD LabView system. The horizontal axis is the position coordinate of the interference fringes, and the vertical axis is the fringe intensity, both in arbitrary units. The threshold intensity is set at 160 on the vertical scale, the threshold fringe width is set at 4 on the horizontal scale, and the threshold number of qualified interference fringes is set at 10, as shown in the T.P.N. box. This scan finds 15 qualified interference fringes as shown in the # Found box. The Warning button lights up whenever the scanned sample satisfies all the three threshold values.

film is so thin that the interference fringes can even be viewed under a white light source, the coherence length of a diode laser, a few centimeters in our case, is more than needed. The diode laser module consists of a 6.4-mW, 670-nm laser diode and an aspheric lens positioned 1 cm in front of the diode. The aspherical lens has a 3-mm-diam aperture, preserving the central part of the laser wavefront and clipping 60% of the laser diode power to make a circular beam. Since the lens aperture only transmits a small portion of the diode-laser wavefront, the laser module produces a 2.5-mW, nearly flattop, circular beam with a half divergent angle of 0.5 mrad in both transverse directions. To expand the laser beam, a 5-cm-focal-length, double-convex lens is installed at a 3-cm distance from the aspherical lens. A 2.5-cm-diam circular laser beam is generated on the image screen. The distance between the diode laser module and the water surface is 22 cm, and that between the water surface and the image screen is 30 cm, as shown in Fig. 6. The laser waist, after the focusing lens, is about 14 cm from the water surface. Therefore the radius of curvature of the laser wavefront is much larger than that of the curved oil edge, which allows us to model the wavefront-splitting interference by using a plane wave and a spherical wave as in the previous section. In our experiment, the laser incident angle is about 75 deg relative to the normal to the water surface. At this incident angle, the laser beam has an elliptical beam profile on the water surface with major axis 3.8 cm and minor axis 1 cm.

In our imaging experiment, we first employed a charge coupled device (CCD) camera as the image extraction system. The CCD signal is connected to a National Instrument IMAQ image capture board installed in a computer. A LabView™ computer code processes the recorded image, and determines whether the image is indeed an interference fringe pattern. In the second phase of our experiment, we replaced the whole imaging and discerning system with a CMOS linear sensor array connected to a compact, home-made logic circuit.

In our CCD-LabView system, a National Instrument IMAQ card captures the CCD image and displays the interference fringes on a computer. We programmed the LabView so that the computer is able to linearly scan the intensity signal both in the vertical and horizontal directions throughout the two-dimensional image. During the scanning process, the program automatically checks three threshold parameters: the fringe intensity, the fringe width, and the number of fringes. The threshold values set the least condition for sending out a warning signal in the event of oil spillage. Checking the fringe intensity ensures that the image signal is above the noise level, and checking the other two parameters guarantees the existence of interference fringes. The linear scan sends out a warning signal whenever it detects a set of interference fringes that satisfies all three threshold values.

Figure 7 shows a typical computer output of our detection system, where the horizontal axis of the window is the position coordinate of a one-dimensional image sample from the CCD camera, and the vertical axis is the intensity of that particular sample. The units are arbitrary. The horizontal line intercepting the intensity signal sets the intensity threshold at 160 on the vertical scale. For this particular case, the threshold fringe width is 4 on the horizontal scale, and the threshold number of qualified interference fringes is 10, as shown in the T.P.N. box. In Fig. 7, the automatic scanning process returns a result of 15 qualified interference fringes, as the # Found box shows. The Warning button lights up whenever the scanned sample satisfies all three threshold values. Our LabView program has full flexibility in presetting the three threshold values, according to the field conditions.

In order to minimize the size and cost, we further replaced the CCD camera and the image-processing computer with a discerning circuit board. The circuit board consists of a Hamamatsu N-MOS linear image sensor (S3923-256Q) and a homemade logic circuit for checking the three threshold parameters given previously. The circuit board is powered by a 5-V dc power supply, and its overall size is similar to a typical computer interface card.

A 250-kHz, 50%-duty-cycle, 2.5-V square wave serves as the master clock of the Hamamatsu image sensor. A 100-Hz, 50%-duty-cycle square wave modulates the 250-

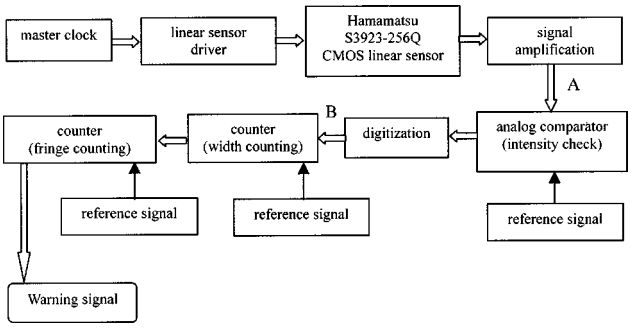

Fig. 8 The data-processing flow chart of our homemade discerning circuit. The interference fringe signal is extracted by a linear array sensor, and then amplified and digitized by subsequent circuit elements. Once the amplified signal passes the check of the three preprogrammed threshold voltage values, the circuit sends out a warning signal of oil spillage.

kHz master clock to separate independent measurements. In each of the 10-ms periods (one cycle of the 100 Hz), the interference intensity information is extracted by the Hamamatsu linear image sensor, amplified in an operational amplifier, and analyzed by three logic stages for threshold value checking. Figure 8 is the data flow chart of our circuit, and Fig. 9 shows the output waveforms at the points *A* and *B* in Fig. 8. The lower trace of Fig. 9 illustrates the amplified interference signal taken by the linear image sensor, corresponding to the point *A* in Fig. 8. The upper trace of Fig. 9 shows the digitized intensity at the points *B* in Fig. 8. The closely packed lines are square waves of the 250-kHz master clock. The digitized intensity is set to 5-V if the signal at the point *A* is higher than the preprogrammed threshold value and is otherwise set to zero. The digitized intensity then goes through two more logic stages to check the fringe width and the number of qualified fringes. If the signal satisfies all the three logic checks, an oil-spillage warning signal is sent to a radio beeper for subsequent action. All the electronics are

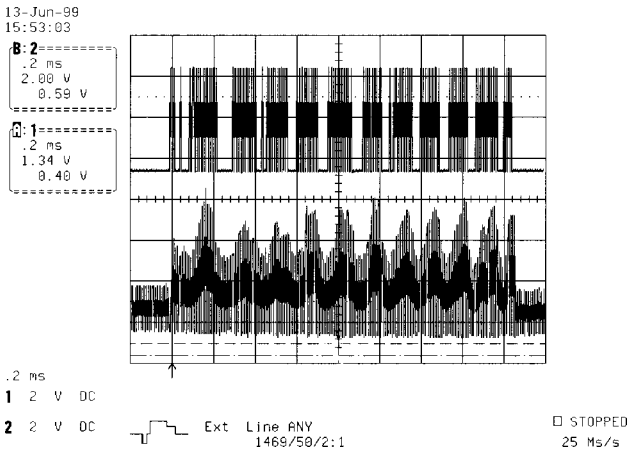

Fig. 9 Typical interference fringe signals before and after digitization. The lower trace shows the amplified fringe signals at the point *A* of Fig. 8. The upper trace is the digitized fringe signal at the point *B* of Fig. 8. A preset voltage provides the threshold value of digitization. The digitized signal is then checked for its fringe width and number of fringes by subsequent circuit elements.

commercial-grade, low-cost, and low-power integrated circuit chips, such as CMOS 4538B, 4047, 4040, 4064, 40174, and the like.

The threshold values are programmable through three reference voltages, according to the field conditions and the optical design. In general, the intensity threshold voltage value can be set at a value slightly higher than the background noise. The background noise is the signal voltage measured without the thin oil film. Our intensity threshold voltage was set 20% above the background noise. The upper limit of the intensity threshold voltage ought to be less than the signal voltage. Typically we have a signal-to-noise ratio larger than two. Optical design determines the threshold values of the fringe width and the number of fringes. For example, if the optics is designed so that the laser incident angle is 75 deg and the laser beam has a full divergence angle of 10 deg, the threshold value of the number of fringes can be ≈ 5 for a TM incident field, as indicated in Fig. 2. We have assumed that the material parameters used in Fig. 2 are still valid for this example. The threshold value of the fringe width is approximately the product of the fringe angular width and the distance between the imaging apparatus and the water surface. For example, near the 75-deg incident angle, the fringe angular width is about 1 deg in Fig. 2, and the fringe spatial width should be ≈ 5 mm for a 30-cm separation between the water surface and the imaging apparatus. If the interference fringes are primarily from wavefront-splitting interference, the threshold values can be inferred in a similar fashion.

In natural water, waves may disturb the signal extraction in a buoyant optical system. If each measurement event is faster than the time constant of water motion, the water surface is considered static by the electronic circuit. Since the surface water wave usually undergoes low-frequency motion, the 100-Hz data-refreshing rate is adequate for most situations. If necessary, the data rate can be increased to avoid the problem of water motion.

We experimentally simulated oil spillage with unleaded gasoline and engine oil in a water tank. The success rate of detecting oil spillage is nearly perfect. The image sensor array circuit performs as well as does the CCD-LabView system. As an early warning system, this technique is designed to provide oil-spill detection before the oil spreads over a large area. Occasional failure occurs when the engine oil forms a thick and smooth layer in the water tank. Under this circumstance, no water-oil interface is available to generate wavefront-splitting interference fringes, and the oil layer is too thick to generate well-separated thin-film interference fringes. However, small air bubbles are often present in the thick oil layer, which are in fact excellent sources of wavefront-splitting interference fringes.

4 Conclusions

We have successfully implemented an optical early-warning system for monitoring oil spillage. The system takes advantage of the thin-film interference and wavefront-splitting interference from the oil and water interfaces. In particular, the wavefront-splitting interference gives excellent fringe visibility even when the refractive indices of water and oil are close to each other. We have tested two detection systems, a CCD-LabView system and a sensor-array–logic-circuit system. Both systems show ex-

cellent reliability and flexibility in discerning the interference fringes resulting from oil slicks. The sensor-array–logic-circuit detection system is compact, low-cost, and low-power, and can be installed in a standalone buoy with ease.

Acknowledgments

The authors thank Ker-Wei Chang for his assistance in the refractive index measurements reported in this paper. This work is supported in part by the National Science Council under contract No. NSC 87-CPC-M-007-012.

References

1. H. A. Espedal and T. Wahl, ''Satellite SAR oil spill detection using wind history information,'' *Int. J. Remote Sens.* **20**(1), 49–65 (1999).
2. D. Flanders, B. M. Sorenson, and C. K. Shen, ''Airborne infrared and ultraviolet remote sensing for oil spill detection,'' *Adv. Imaging* **12**(4), 55–57 (1997).
3. V. Wismann, ''Radar signatures of mineral oil spills measured by an airborne multifrequency radar and the ESR-1 SAR,'' in *IEEE Proc. International Geoscience and Remote Sensing Symp.*, Vol. 3, pp. 940–942 (1993).
4. A. H. Schistad Solberg and R. Solberg, ''Large scale evaluation of features for automatic detection of oil spills in ERS SAR images,'' in *IEEE Proc. International Geoscience and Remote Sensing Symp.*, Vol. 3, pp. 1484–1486 (1996).
5. K. W. Bjerde, A. H. Schistad Solberg, and R. Solberg, ''Oil spill detection in SAR Imagery,'' in *IEEE Proc. International Geoscience and Remote Sensing Symposium*, Vol. 3, pp. 943–945 (1993).
6. M. Barni, M. Betti, and A. Mecocci, ''Fuzzy approach to oil spill detection on SAR image,'' in *IEEE Proc. International Geoscience and Remote Sensing Symp.*, Vol. 1, pp. 157–159 (1995).
7. A. H. Schistad Solberg, G. Storvik, R. Solberg, and E. Volden, *IEEE Trans. Geosci. Remote Sens.* **37**(4), 1916–1924 (1999).
8. C. J. Fleck and M. J. Sweeney, ''Oil spillage detector,'' U.S. Patent No. 5,481,904 (1996).
9. H. R. Gram, M. P. Jadamec, and J. W. Jonathan, ''Oil spill detection system,'' U.S. Patent No. 5,461,236 (1995).
10. A. Jacobson, ''Automatic detection system of oil spillage into sea waters,'' U.S. Patent No. 5,208,465 (1993).
11. E. Hecht, *Optics*, 3rd ed., p. 412, Addison-Wesley (1998).
12. E. Hecht, *Optics*, 3rd ed., pp. 112–113, Addison-Wesley (1998).
13. E. Hecht, *Optics*, 3rd ed., p. 384, Addison-Wesley (1998).
14. B. E. A. Saleh and M. C. Teich, *Fundamentals of Photonics*, p. 49, Wiley (1991).

Yen-Chieh Huang completed his BS degree in 1987 in the Electrical Engineering Department, National Sun Yat-Sen University, Taiwan. He then received his MS degree in 1991 and PhD in 1995, both from the Electrical Engineering Department, Stanford University. During February 1997 and July 1999, he was an assistant professor in the Department of Atomic Science, National Tsinghua University, Taiwan. Dr. Huang is currently an assistant professor with the Department of Electrical Engineering at the same university. His research interests include optical environmental technology, nonlinear laser frequency conversion, and laser-driven electron acceleration.

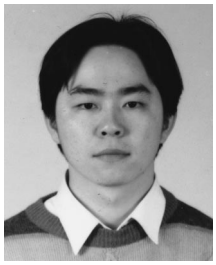

Uen-Chin Liang received his BS degree in 1997 and MS degree in 1999 from the Department of Atomic Science, National Tsinghua University, Taiwan. He completed his masters dissertation with a novel electronic design for an interferometric oil-spill warning system.